Multi-Radiation Center Transmitter Models for Ray Tracing

Robert Brem, *Student Member, IEEE*, and Thomas F. Eibert, *Senior Member, IEEE*

***Abstract*—Concepts to improve transmitter models for electromagnetic ray tracing are investigated. The goal is to increase the accuracy of radiated field prediction in the near-field region of the radiator while the ray-based field representation is retained. Basic idea is to divide the radiating structure in smaller parts and treat them as subtransmitters, instead of using only one single transmitter, which is common practice. Not only antenna elements are considered, but also their surroundings, i.e., objects in close proximity such as a carrier platform. In order to generate the subtransmitter models for ray tracing, the current distributions on the radiating structure are computed by an multilevel fast multipole method (MLFMM) integral equation solver and the subtransmitters are directly obtained from the hierarchical multilevel plane wave representation within the MLFMM. Numerical results demonstrate the improved modeling accuracy.**

***Index Terms*—Integral equation solver, multilevel fast multipole method (MLFMM), near-field, ray tracing, subtransmitter.**

I. Introduction

RAY TRACING based on geometrical optics (GO) and its extensions Geometrical Theory of Diffraction (GTD) or Uniform Theory of Diffraction (UTD) [1] is an important and widely used technique to determine electromagnetic fields in large scenarios, where computations with full-wave solvers would not be feasible due to complexity. Consider e.g., the planning of mobile networks in urban regions or indoor scenarios. During the last decades this method has been used extensively. Besides the applicability to large objects and distances, a main advantage is the absence of run-time and memory penalties due to increasing frequency. So, ray tracing has been successfully applied to problems far beyond 50 GHz (e.g., [2]). The computational costs are generally much lower for ray tracing than for rigorous numerical methods. Another advantage is the easy parallelization [3], [4]. In many publications ray tracing has been used for performance evaluations of radio links [5]–[8]. Typically, reflections and diffractions are considered for the interaction with objects lying in the ray path, but more complex models can also take transmission through penetrable objects into account [9].

Two methods are commonly used: The first is deterministic ray tracing, where all relevant ray paths between transmitter and receiver location are computed exactly. This method is time-consuming for complex scenarios with many interactions. The second method is ray launching, also called shooting and bouncing rays (SBR)-technique [10], where rays are sent out in arbitrary directions and no time-consuming preprocessing is required. However, the results of both approaches are equal only if the number of rays in the SBR method is large enough to cover all relevant propagation paths. In order to limit the computational effort, rays in SBR are neglected after a preset number of interactions or a certain attenuation. Rays are detected if they hit a sphere circumscribing the receiver location [11]. Typically, a transmitter is modeled as a point source from which all energy is radiated by spherical waves. If the distance to the receiver location and to intersecting objects is large enough, this is an appropriate model which gives good results. The well-known far-field-condition should at least be fulfilled. For decreasing distances, field computations become more and more inaccurate due to phase errors, so that a simple point source model is not a good choice any more. This can be a quite restrictive requirement when fields shall be computed in the near-field region of a transmitter which is not a small object or if reflecting or diffracting objects are close to the transmitter. Consider the utilization of ray tracing to characterize radio links in indoor environments, or e.g., a car with antennas in a tunnel. Ray tracing in indoor environments has been used for a long time. However, little attention has been paid on compliance with the far-field condition, which is a basic requirement for ray propagation. Normally, only one point source is used for the transmitter.

In this paper, it is shown how improved transmitter models can be generated for ray tracing simulations. The goal is to increase the accuracy of near-field representations without losing the simplicity of ray tracing, which is based on the simple structure of far-fields. The antennas, e.g., a multiple-input multiple-output (MIMO) antenna array, and also their near environment which influences the radiation characteristic is taken into account. This is achieved by partitioning the transmitter and its close environment into subdomains, where the radiation of every subdomain is represented by a single radiation center and the radiation centers have fixed amplitude and phase relations with respect to each other. So, every radiation center can be treated by ray tracing and the field representation remains still valid nearby the radiation structure. E.g., for vehicular antennas, the whole vehicle or parts of it can be treated as part of the transmitter, whose radiation is represented by multiple related radiation centers. In contrast to the hybrid methods presented in [12] and [13], where ray tracing based on GO and UTD was employed to extend the applicability of integral

Manuscript received September 20, 2011; revised January 03, 2012; accepted February 25, 2012. Date of publication May 01, 2012; date of current version July 02, 2012.

The authors are with Lehrstuhl für Hochfrequenztechnik, Technische Universität München, 80290 Munich, Germany (e-mail: hft@ei.tum.de).

Color versions of one or more of the figures in this paper are available online at http://ieeexplore.ieee.org.

Digital Object Identifier 10.1109/TAP.2012.2196956

equation and finite-element models to larger scale scenarios, in this paper ray tracing is the core of the formulation and the applicability of ray tracing will be extended to smaller scale scenarios.

The paper is organized as follows. In Section II, the foundation of the modeling approach is developed. Section III gives a validation by comparison between exact and ray tracing results. Section IV shows options to simplify and improve these models. Finally, a short conclusion is given.

II. Modeling Approach

Consider the electric field $\boldsymbol{E}$ of an electric source current density $\boldsymbol{J}$ according to [1]

$$\boldsymbol{E}(\boldsymbol{r}) = -jkZ \iiint_V \left(\overline{\boldsymbol{I}} + \frac{1}{k^2}\nabla\nabla\right) \frac{\mathrm{e}^{-jk|\boldsymbol{r}-\boldsymbol{r'}|}}{4\pi\,|\boldsymbol{r}-\boldsymbol{r'}|} \cdot \boldsymbol{J}(\boldsymbol{r'})\,dv' \tag{1}$$

where a time factor $\mathrm{e}^{j\omega t}$ is assumed and suppressed. $k = \omega\sqrt{\varepsilon\mu}$ is the wave number and $Z = \sqrt{\mu/\varepsilon}$ is the characteristic impedance of the considered homogeneous medium (typically free space), respectively. Under far-field conditions, i.e., for $r = |\boldsymbol{r}| \gg |\boldsymbol{r'}| = r'$, this expression simplifies into

$$\boldsymbol{E}^{FF}(\boldsymbol{r}) = -jkZ\frac{\mathrm{e}^{-jkr}}{4\pi\,r} \underbrace{(\overline{\boldsymbol{I}} - \hat{r}\hat{r})}_{(\hat{\vartheta}\hat{\vartheta}+\hat{\varphi}\hat{\varphi})} \cdot \iiint_V \mathrm{e}^{jk\hat{r}\cdot\boldsymbol{r'}} \boldsymbol{J}(\boldsymbol{r'})\,dv' \tag{2}$$

where $\hat{r}$ is the unit vector in direction of $\boldsymbol{r}$. It is well known that such far-fields with spherical wave fronts are locally plane waves and its amplitude can be obtained by energy considerations. Also, these fields can be taken as sources of ray tracing approaches according to GO or GTD/UTD, where they are a special form of the more general astigmatic ray representation according to [1]

$$\boldsymbol{E}^R(s) = \mathrm{e}^{-jks}\sqrt{\frac{\rho_1\rho_2}{(\rho_1+s)(\rho_2+s)}}\boldsymbol{E}_0(0) \tag{3}$$

valid along a straight ray path parameterized by s. ρ_1, ρ_2 are the radii of curvature of the astigmatic ray tube. Since (1) does not have ray field character, it is clear that ray tracing approaches are feasible only in the far-field of radio transmitters. Utilizing the fast multipole method (FMM) representation of the electric field Green's function, (1) can however be written in the form of [14], [15]

$$\boldsymbol{E}(\boldsymbol{r}) = \lim_{L\to\infty} \oiint T_L(\hat{k},\boldsymbol{r})\boldsymbol{E}^{FF}(r\hat{k})\,d^2\hat{k} \tag{4}$$

with the translation operator T_L according to [14]

$$T_L(\hat{k},\boldsymbol{r}) = \frac{jk}{4\pi}\sum_{l=0}^{L}(-j)^l(2l+1)\mathrm{h}_l^{(2)}(k|\boldsymbol{r}|)\mathrm{P}_l(\hat{k}\cdot\hat{r}) \tag{5}$$

and under the assumption of $r > \max(r')$. The term $\mathrm{h}_l^{(2)}$ refers to the second kind spherical Hankel function of degree l and P_l is the Legendre polynomial of degree l. With this representation, it is clear that the far-field of a source distribution contains also the complete near-field information as long as the observation points $\boldsymbol{r}$ are chosen outside of the source region. However, in a conventional ray tracing approach with energy conserving ray fields and following Fermat's principle it is not possible to access this near-field information. In order to overcome this issue and make the ray-tracers applicable in the near-field of a source distribution, a way must be found to access the near-field information in the form of ray tracing compatible far-field representations. It is well-known that the transition from near- to far-field region of a transmitter depends on its dimension. The typical condition for the far-field is $r > 2D^2/\lambda$ (with distance r, max. extension D of radiator and wavelength λ) [16]. When the dimension of the radiator is smaller, the far-field starts at a smaller distance to it. Therefore, the goal is to subdivide the entire radiating object into smaller subtransmitters. For each of them, the far-field condition is fulfilled at a smaller distance compared to the complete transmitter so that we can assume locally plane waves and apply ray tracing. This approach enables a ray based far-field representation of the transmitter's near-field.

In order to compute electromagnetic fields, it is useful to determine an equivalent current distribution in a first step. For this, fast integral equation solvers like the efficient MLFMM algorithm are used by default, but other full-wave methods could be used as well. MLFMM [14], [15], [17] is ideally suited for the generation of smaller radiators (subtransmitters) because it is based on a hierarchical subdivision of the object into levels, where each level contains a different number of groups or boxes (cubes) representing a part of the object. The entire object is enclosed in a hierarchical oct-tree of boxes with different sizes on the different levels. Instead of computing the interaction of each current with each other current, as done in the classical method of moments (MoM), hierarchical plane wave representations of the radiated and received fields, which are related by appropriate translation operators [14], are employed for an efficient interaction computation.

The same efficient hierarchical scheme can be employed for the computation of the electromagnetic fields (near-fields and far-fields) from a known current distribution, e.g., in form of a postprocessing step of an integral equation solution [13]. For all MLFMM boxes or subtransmitters on the lowest level (smallest boxes), the computed currents are used to generate a plane wave representation of the corresponding radiated fields [15]. Eight subtransmitter boxes with their fields are combined to one new subtransmitter on the next higher level with double box side length and new source point in the middle of the eight smaller ones as illustrated in Fig. 1. This is done by an aggregation and interpolation operation. By continuing this procedure, the simplest transmitter model with only one source point for the entire object is obtained as the single box on the highest level. In order to generate transmitter models for ray tracing, all subtransmitters of one level, representing in sum the entire object, are chosen. For each of them, field samples on a spherical grid are computed from the plane wave representation. These field samples serve as start values $\boldsymbol{E}_0$ in (3). By adjusting the size of the lowest level boxes and choosing the subtransmitters of a certain level, great freedom exists in changing dimension and number of the transmitter models for ray tracing. Adaptive subtransmitter models can be easily generated by switching to different level representations dependent on the particular requirements.

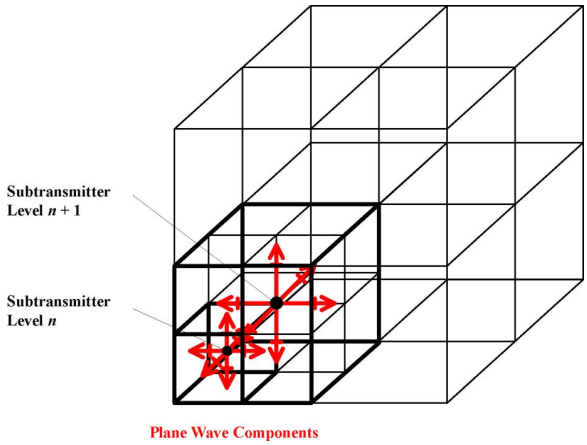

Fig. 1. Plane wave components of eight subtransmitters at level n are used to compute the plane wave representation for the corresponding higher subtransmitter at level $n+1$.

Often, only the far-field radiation characteristic of an antenna system is given, e.g., for a commercial antenna. By solving the inverse problem according to (2), an equivalent current distribution $\boldsymbol{J}$ on an arbitrary surface can be computed [18], [19]. Afterwards, near-fields or subtransmitter far-fields as required for the proposed ray tracing procedure with subtransmitters can be computed as described before.

An important aspect is also the numerical complexity of the subtransmitter approach. Prior to the start of the ray tracing simulations, the far-fields for the individual subtransmitters must be determined. These far-fields are typically obtained from equivalent currents, which are normally found by MoM-based methods, i.e., classical MoM or inverse current methods or enhanced multilevel FMM with its well-known complexities [14]. The far-field computation from the equivalent currents requires usually considerably less time than the solution for the currents. Again, MLFMM acceleration is the optimum choice and the far-fields for the subtransmitters are obtained without any extra cost within the hierarchical far-field computation of the complete radiating structure.

The complexity of the ray method depends on its type. Ray launching has a complexity of $\mathcal{O}(N_{Tx}N_RN_IN_W)$, where N_{Tx} is the number of subtransmitters, N_R represents the total number of sent rays per subtransmitter, N_I is the maximum number of intersections and N_W denotes the number of walls or simply areas, which have to be checked for intersection. To N_R belong all rays propagating in directions for which reception is possible, i.e., they are sent out in a properly chosen angular region. The complexity of deterministic ray tracing with N_{Rx} receivers is $\mathcal{O}(N_{Tx}N_{Rx}N_W^{N_I})$, see [20]. The exponential dependency on the number of intersections shows that the ray launching (SBR) approach can easily outperform deterministic ray tracing in terms of computational efficiency for large problems. Space partitioning or visibility checks help to accelerate both ray methods by holding the number of required intersection tests per ray low. This is essential for large problems since intersection tests need most of the CPU time. As presented, the numerical complexity of the subtransmitter approach increases linearly with the number of transmitters, due to typically identical processing steps for every subtransmitter.

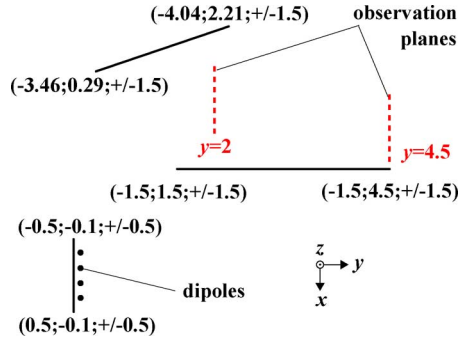

Fig. 2. Field measurement near PEC plates (top view), dimensions in m.

III. Validation of the Approach

For the simulations, basically two approaches are used. To compute the currents on the transmitting structure and produce the far-field samples of the desired subtransmitters on a certain level, an MLFMM integral equation solver is employed [15], [17], [21]. In addition to many setting options like solving method, accuracy, etc., the minimum box size can be adjusted. Then, the field information is used as input for an SBR ray-tracer [22], [23] which computes the electric field at a point in space as superposition of all transmitter ray contributions by consideration of reflections. In order to achieve accurate results, the techniques proposed in [24] have been implemented.

Consider the following scenario shown in Fig. 2. Four dipole antennas with length 12 cm and spacing 5 cm in z-direction are placed 10 cm in front of a PEC (perfect electric conductor) reflector plate with dimensions 1 m $\times$ 1 m lying in the xz-plane. The dipoles are excited in its centers with 2.5 GHz voltage sources of 1 V. A few meters away two large PEC plates are placed. For the exact simulation with the integral solver the plates are discretized with triangles of side length $\lambda/10$. The complex electric field is computed in two 1 m $\times$ 1 m planes, where the plane at $y = 2$ m is partially in the line-of-sight (LOS) and reaches from $x = -3$ to -2 m whereas the plane at $y = 4.5$ m is not seen from the radiator and reaches from $x = -2.6$ to -1.6 m. The extent in z-direction is -0.5 to 0.5 m for both planes. The spacing of the probe points is 2 cm, so that a total of 2601 (51 $\times$ 51) field values are computed within each observation plane. In order to generate the input data for the ray-tracer, only the dipoles together with the reflector plate are simulated with the integral equation solver. With the same excitation as before, the electric far-field is computed for different sets of subtransmitters. With this data, now the ray-tracer is used to determine the fields in the two planes under consideration of reflection and diffraction. Fig. 3 compares the results for the plane at $y = 2$ m. In the upper subfigures, the computed powers of integral equation solver (exact) and ray-tracer are shown along a cut at $z = 0$ m. The lower subfigures show the maximum error observed in the observation plane for fixed x-values, i.e., x fixed and z assumes the values for the maximum error. As can be seen, the results are in better agreement with increasing number of subtransmitters. A measure for the total error can be given by the mean square error

$$\sigma\,[\mathrm{dB}] = \sqrt{\frac{1}{N}\sum_{i=1}^{N}\left(\left|\boldsymbol{E}_R^i\right|\,[\mathrm{dB}] - \left|\boldsymbol{E}_0^i\right|\,[\mathrm{dB}]\right)^2} \qquad (6)$$

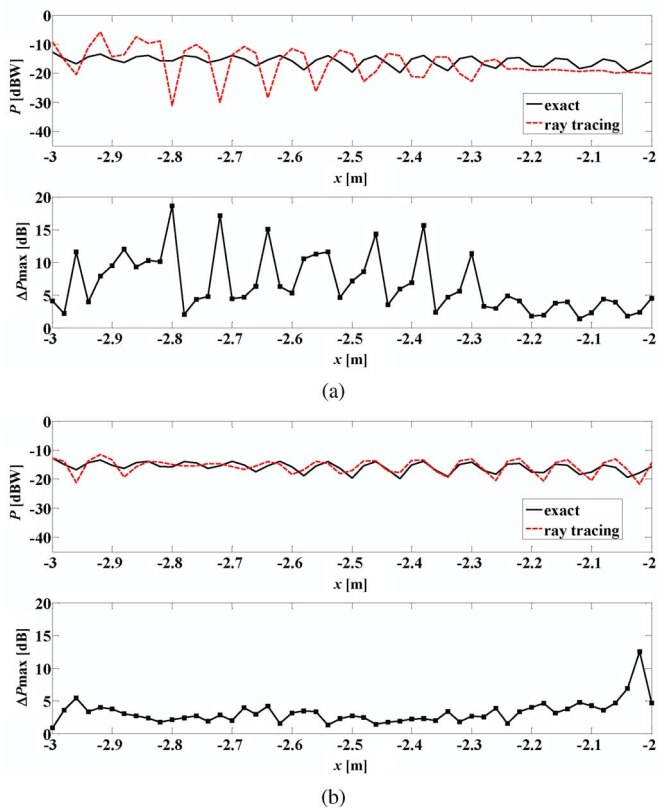

Fig. 3. Comparison of ray tracing simulation with exact field computation for the plane $y = 2$ m in Fig. 2. Upper subfigure: comparison of powers along horizontal cut of observation plane $z = 0$ m. Lower subfigure: maximum error for x fixed and z variable. (a) One (sub)transmitter. (b) Four subtransmitters.

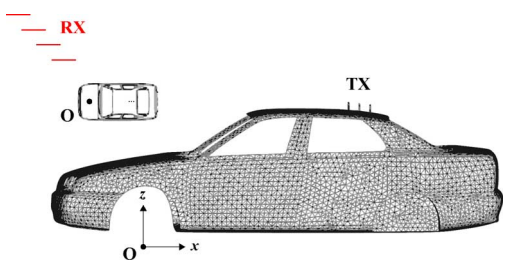

Fig. 4. Car with roof antenna.

where N is the number of observation points, and $|E_R^i|$ and $|E_0^i|$ are the ith magnitude (in dB) of the electric field computed by ray tracing and by the integral solver (reference), respectively. This error gives the following results: $\sigma(1 \text{ subtransmitter}) = 5.27$ dB and $\sigma(4 \text{ subtransmitters}) = 2.04$ dB.

The simulation results in the plane at $y = 4.5$ m show that there is practically no difference between using one subtransmitter and four subtransmitters. The distance is large enough to describe the fields with only one point source properly. By using the dimension $D = \sqrt{2}$ m and $\lambda = 12$ cm, one would get a minimum distance of 33 m to apply the far-field approach. However, due to the fact that the induced currents on the reflector plate decay quickly, the effective far-field distance is much smaller.

In the next example, the field of a car antenna is simulated. As shown in Fig. 4, three monopoles are mounted on the back of the roof. Each of them is of length 8.3 cm and the spacing is 10 cm. The monopoles are fed by 900 MHz voltage sources. The

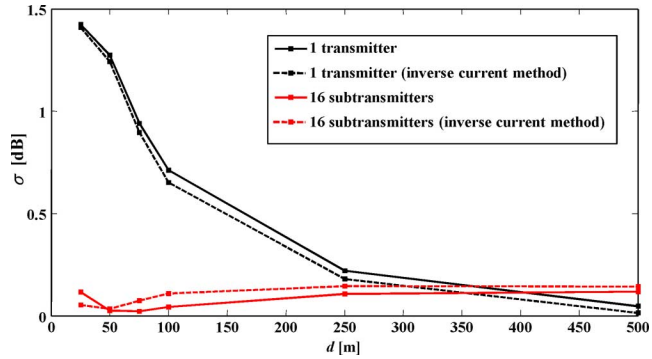

Fig. 5. Error in field computation for different numbers of transmitters and distances, where the car model in Fig. 4 has been utilized.

field in free space is computed at different distances d from the origin of the coordinate system (s. Fig. 4). Once again, receiver planes with 1 m^2 are used. They all lie in the xz-plane and are arranged along the line $y = -x$ and $z = 10$ m. The electric field is computed with the integral equation solver and with the ray-tracer, where one subtransmitter and 16 subtransmitters are used. The error compared to the integral equation solver solution is again computed by (6), for six receiver planes as indicated in Fig. 4 (four planes drawn). The results for the errors are depicted in Fig. 5 dependent on the distance to the centers of the receiver planes. As expected, near to the car, more subtransmitters improve the accuracy significantly, far away from the car both models produce the same accurate results.

The inverse current method as discussed before is also applied for this simulation example. First, the current distribution on the car is determined from the given far-field. Then subtransmitter far-fields are computed and the ray tracing is performed. The error curves in Fig. 5 show the good performance, where the slight deviations are due to the stochastic ray launching.

IV. Simplification and Improvement of the Models

In order to reduce simulation time for ray tracing, a simple way would be to neglect all subtransmitters which radiate considerably less energy than others. Fig. 6 shows a very fine model of the car in Fig. 4 with 84 subtransmitters. The value m in dB is the ratio between the maximum E-field magnitude of a subtransmitter and the maximum E-field magnitude of all subtransmitters. In the right figure, all subtransmitters with $m < -26$ dB are neglected, so that 52 subtransmitters remain. Both models are used in the scenario shown in Fig. 7, where the electric field magnitude shall be determined at the roof of one building at RX1 and around the corner at RX2. The buildings are treated as PEC objects. The field prediction results for the two subtransmitter models and for a third model with only 34 subtransmitters are shown in Table I.

Obviously, this method can speed up the simulation, here by a factor of 1.6 for the reduction to 52 transmitters, without introducing noticeable errors. Using only 34 transmitters is not reasonable any longer. This simplification should only be used, when the maximum field strengths of the subtransmitters differ strongly, i.e., there are very weakly radiating subtransmitters.

Until now, the center of each subtransmitter box was used as the radiation center. In general, this is not the best choice. It is obvious that the phase error in ray tracing is low, when the rays

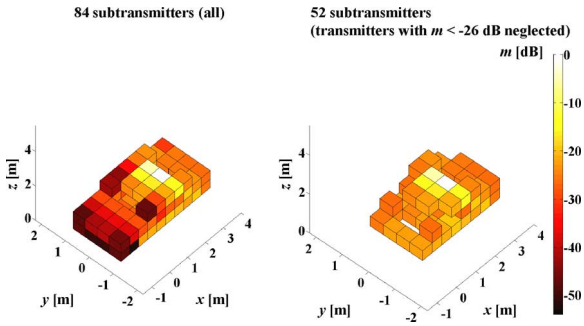

Fig. 6. Neglect of weak radiating subtransmitters in a car model.

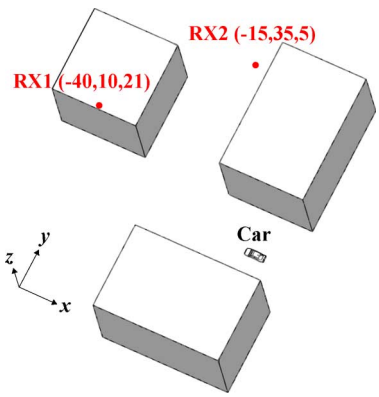

Fig. 7. Simple scene for a ray tracing test: Car surrounded by buildings. Dimensions in m.

TABLE I
ELECTRIC FIELD MAGNITUDES AT DIFFERENT RECEIVER LOCATIONS

subtransmitters	RX1(-40.0 10.0 21.0)m	RX2(-15.0 35.0 5.0)m
84	0.0158 V/m	0.0132 V/m
52	0.0164 V/m	0.0165 V/m
34	0.0181 V/m	0.0224 V/m

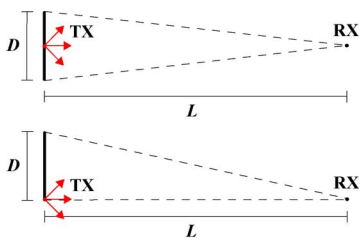

Fig. 8. Different choices for the radiation center of a current-carrying plate.

start propagating from a point preferably near to the location of the main current contribution. Consider Fig. 8, where a current-carrying object, here a plate with length D, produces an electric field at far-field point RX at distance L. The radiation center in the middle, as in the upper figure, is the best choice because the maximum phase difference in RX due to the currents on the edges, is minimized. With the known requirement that this phase difference should be smaller than $\pi/8$ for the far-field, the condition $L > 2D^2/\lambda$ follows. The bad choice to position the radiation center at one edge of the plate, as shown in the second figure, would require $L > 8D^2/\lambda$ to keep the phase error below $\pi/8$.

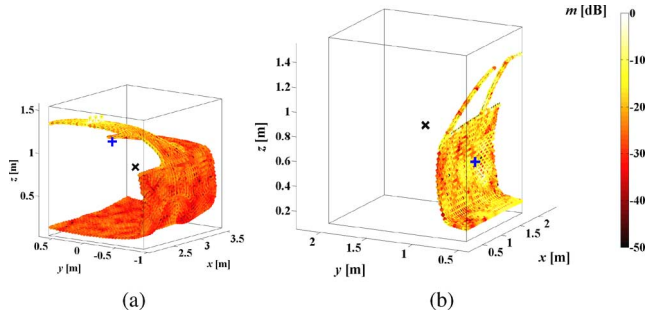

Fig. 9. Current distribution in subtransmitter boxes with box centers (×) and gravitational centers of currents (+) which serve as new radiation centers. (a) Back. (b) Door.

In order to determine a better radiation center for the subtransmitters, the computed current coefficients and their position are used in order to compute the weighted average position (gravity center)

$$\boldsymbol{r} = \frac{\sum_{i=1}^{N} w_i \boldsymbol{v}_i}{\sum_{i=1}^{N} w_i} \qquad w_i = \frac{I_i}{\max_i (I_i)} \tag{7}$$

where N is the number of current basis functions in the subtransmitter, $\boldsymbol{v}_i$ is the edge midpoint of the current basis function i and the weights w_i are computed as current magnitude I_i over maximum current of the subtransmitter. For the postprocessing field computation within the MLFMM, these locations are used as new source points. In Fig. 9 two subtransmitter boxes of side length 1.5 m, containing currents of the car, are shown. The currents are normalized with respect to the maximum value and visualized in logarithmic scale. It can be clearly seen that the new radiation centers lie close to the main current contribution.

In Fig. 10 the phase of the electric field component E_z in receiver planes of 1 m^2 at $x = -15$ m and $y = 15$ m is compared to the exact one. The car model of Fig. 4 with eight subtransmitters is used. In the left figures, the center of each of the eight subtransmitters is used as radiation center, whereas the gravitational centers of the currents give the much better results shown on the right.

For the next investigation, a spherical multipole expansion in form of [25]

$$\boldsymbol{E}^{FF} = \frac{\mathrm{e}^{-jkr}}{kr} \sum_{l=1}^{L} \sum_{m=-l}^{l} j^l \left(-a_{lm}\boldsymbol{n}_{lm} + Z b_{lm}\boldsymbol{m}_{lm}\right) \tag{8}$$

with

$$\begin{aligned} \boldsymbol{n}_{lm} &= \boldsymbol{e}_\theta \frac{\partial Y_{lm}}{\partial \theta} + \boldsymbol{e}_\phi \frac{1}{\sin\theta} \frac{\partial Y_{lm}}{\partial \phi} \\ \boldsymbol{m}_{lm} &= -\boldsymbol{e}_\theta \frac{1}{\sin\theta} \frac{\partial Y_{lm}}{\partial \phi} + \boldsymbol{e}_\phi \frac{\partial Y_{lm}}{\partial \theta} \end{aligned} \tag{9}$$

is employed. Here, k is the wave number, Z the free-space wave impedance, L is the multipole order and Y_{lm} are spherical harmonics. The amplitudes a_{lm} and b_{lm} have to be determined. Consider a Hertzian dipole which is placed at the center of a subtransmitter box. With the electric field referred to the box

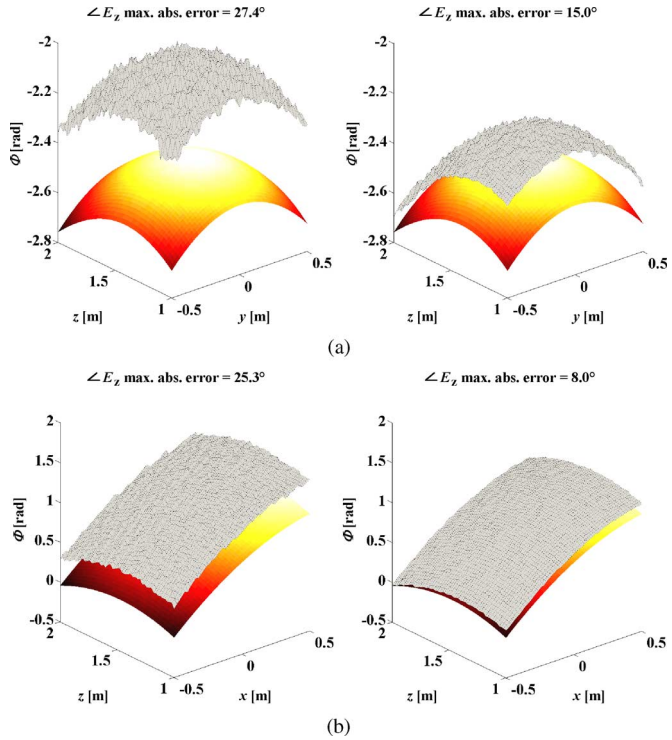

Fig. 10. Reduced phases errors due to radiation center optimization (gray: ray tracing simulation). Utilization of the car model in Fig. 4 with eight subtransmitters. (a) Plane at $x = -15$ m. (b) Plane at $y = 15$ m.

center as origin of the spherical coordinate system, the amplitudes can be computed and only for $l = 1$, nonzero values will be obtained. When this dipole is placed somewhere outside the center, but the box center remains the origin, also amplitudes with $l > 1$ will be nonzero. From the view of this center, a part of the electric power is now distributed over higher multipoles. The overall electric power must be constant, no matter where the dipole has been placed. This means, except for a small error due to the finite series, a summation of all power contributions of the multipoles must converge towards the total power value within the correctly chosen multipole order L (dependent on the size of a subtransmitter box). These observations can be used to search for improved radiation centers for a complex current distribution within a subtransmitter box. The smaller the multipole order for which the cumulative sum of multipole powers reaches the total power value, the better is the applicability of the reference point as source point. With (9) the normalized power can be computed as

$$P = \sum_{l=1}^{L} l(l+1) \sum_{m=-l}^{l} \left(|a_{lm}|^2 + Z^2 |b_{lm}|^2 \right). \qquad (10)$$

This method is applied on the previous car model with 16 subtransmitters. For 512 equally spaced test points within each box, the multipole amplitudes are computed. Then, the cumulative power is computed for each point. Fig. 11 shows the curves for one subtransmitter, plotted over the multipole order l (maximum $L = 19$).

The point in each box, where the corresponding power curve reaches 90% of the total power at lowest l, is taken as radiation center. Then, ray tracing is used to determine the

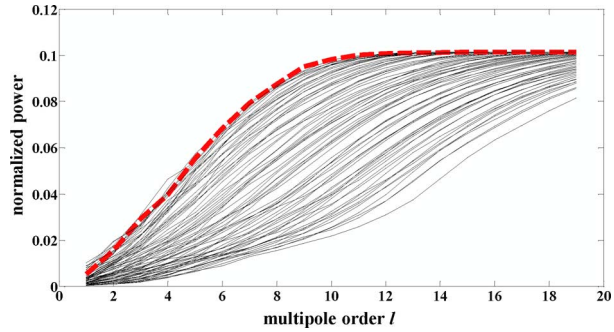

Fig. 11. Normalized cumulative power curves for some of the 512 test points in one subtransmitter box. The red curve reaches the power maximum at lowest l.

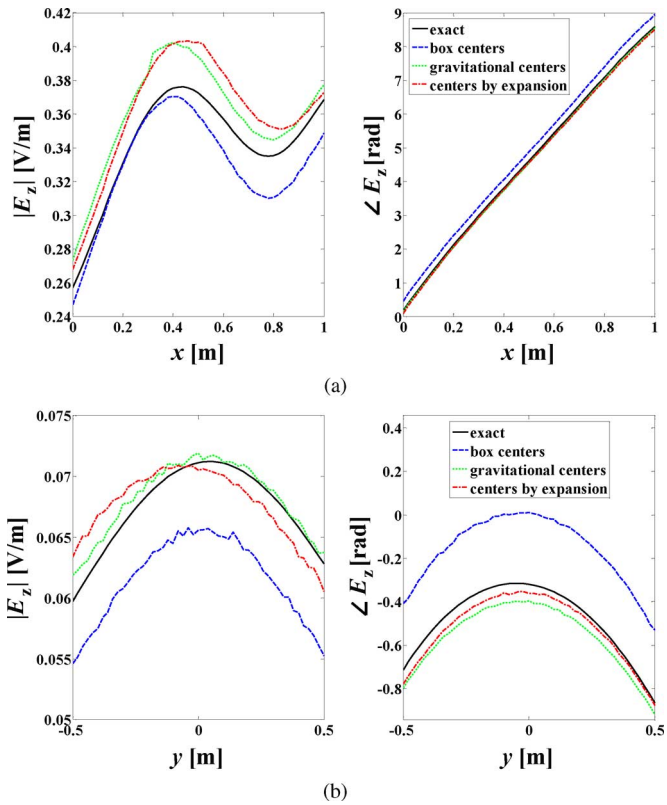

Fig. 12. Electric field component E_z for the car model in Fig. 4. (a) Along line $(0 \ldots 1, 3, 3)$ m. (b) Along line $(-3, -0.5 \ldots 0.5, 3)$ m.

z-component of the electric near-field of the transmitters at line $(0 \ldots 1, 3, 3)$ m and $(-3, -0.5 \ldots 0.5, 3)$ m. Fig. 12 shows the results. Also the curves for exact solution by the integral equation solver and for ray tracing with box centers and gravitational centers (according to (7)) as source points are shown.

Obviously, the multipole expansion to search for improved radiation centers delivers good results. However, for the considered example the results are not better than those of the aforementioned simple method according to (7). This can be expected from the smooth run of the power curves in Fig. 11.

V. Conclusion

In this paper, a method to expand the range of application for electromagnetic ray tracing to the near-field region of a radiating object was shown. The MLFMM is used to produce subtransmitters from the radiating structure. In a first step, the currents

on the surface of the object are efficiently computed. In a post-processing step, the electromagnetic field distribution for each subtransmitter is determined by using the currents in the corresponding subtransmitter box. The algorithm is based on a hierarchical scheme, where the subtransmitter boxes belong to levels and all subtransmitter boxes of one level contain the whole object and have the same size. Eight subtransmitters of one level are aggregated to a new subtransmitter of the next higher level. By adjusting the size of the lowest level subtransmitter boxes and choosing the desired level, great freedom exists in generating the transmitter models for ray tracing. It was shown that the multi-transmitter approach improves the accuracy of field computation in the near-field region of the radiator because this near-field can be accurately expressed by a ray-based far-field representation of smaller subtransmitters. The performed simulations show very good results. Options for model simplification and improvement were presented.

ACKNOWLEDGMENT

The authors gratefully acknowledge the support of the TUM Graduate School's Faculty Graduate Center Electrical Engineering and Information Technology (FGC-EI), Technische Universität München.

REFERENCES

[1] C. Balanis, *Advanced Engineering Electromagnetics*. New York: John Wiley & Sons, 1989.
[2] C. Algiannakis, I. Robertson, and A. Aghivami, "A 3D raytracing model for the study of sectored antenna performance in indoor radio communications systems," in *Proc. 6th IEEE Int. Symp. Personal, Indoor Mobile Radio Commun.*, Sep. 1995, vol. 2, pp. 414–418.
[3] B. Epstein and D. Rhodes, "GPU-accelerated ray tracing for electromagnetic propagation analysis," presented at the IEEE Int. Conf. Wireless Inf. Technol. Syst., Honolulu, HI, Sep. 2010.
[4] S. Bai and D. Nicol, "Acceleration of wireless channel simulation using GPUs," in *Proc. Eur. Wireless Conf.*, Apr. 2010, pp. 841–848.
[5] K. Dandekar, A. Arredondo, G. Xu, and H. Ling, "Computational electromagnetic simulation of smart antenna systems in urban microcellular environments," *IEEE Trans. Veh. Technol.*, vol. 52, no. 4, pp. 733–742, Jul. 2003.
[6] R. Hoppe, G. Wölfle, H. Buddendick, and F. Landstorfer, "Fast planning of efficient WCDMA radio networks," in *Proc. IEEE 54th Veh. Technol. Conf.*, Oct. 2001, vol. 4, pp. 2721–2725.
[7] H. Buddendick, G. Wölfle, S. Burger, and P. Wertz, "Simulator for performance analysis in UMTS FDD networks with HSDPA," in *Proc. 15th IEEE Int. Symp. Personal, Indoor Mobile Radio Commun.*, Sep. 2004, vol. 3, pp. 2251–2255.
[8] S. Burger, H. Buddendick, G. Wölfle, and P. Wertz, "Location dependent CDMA orthogonality in system level simulations," in *Proc. IEEE 61st Veh. Technol. Conf.*, May 2005, vol. 1, pp. 419–423.
[9] S. Grubisic, W. Carpes, C. Lima, and P. Kuo-Peng, "Ray-tracing propagation model using image theory with a new accurate approximation for transmitted rays through walls," *IEEE Trans. Magn.*, vol. 42, no. 4, pp. 835–838, Apr. 2006.
[10] I. Kelly, G. Benavides, R. Bhalla, H. Ling, W. Vogel, and H. Foltz, "Urban channel propagation modeling using the shooting and bouncing ray technique," in *Proc. IEEE Antennas Propag. Soc. Int. Symp.*, Jul. 1997, vol. 3, pp. 2018–2021.
[11] J. Parsons, *The Mobile Radio Propagation Channel*. Hoboken, NJ: Wiley, 2000.
[12] A. Tzoulis and T. Eibert, "A hybrid FEBI-MLFMM-UTD method for numerical solutions of electromagnetic problems including arbitrarily shaped and electrically large objects," *IEEE Trans. Antennas Propag.*, vol. 53, no. 10, pp. 3358–3366, Oct. 2005.
[13] A. Tzoulis and T. Eibert, "Efficient electromagnetic near-field computation by the multilevel fast multipole method employing mixed near-field/far-field translations," *IEEE Antennas Wireless Propag. Lett.*, vol. 4, pp. 449–452, Dec. 2005.
[14] W. Chew, J. Jin, E. Michielssen, and J. Song, *Fast and Efficient Algorithms in Computational Electromagnetics*. Boston, MA: Artech House, 2001.
[15] T. Eibert, "A diagonalized multilevel fast multipole method with spherical harmonics expansion of the k-space integrals," *IEEE Trans. Antennas Propag.*, vol. 53, no. 2, pp. 814–817, Feb. 2005.
[16] R. Johnson, *Antenna Engineering Handbook*. New York: McGraw-Hill, 1993.
[17] T. Eibert, "Some scattering results computed by surface-integral-equation and hybrid finite-element-boundary-integral techniques, accelerated by the multilevel fast multipole method," *IEEE Antennas Propag. Mag.*, vol. 49, no. 2, pp. 61–69, Apr. 2007.
[18] T. Eibert and C. Schmidt, "Multilevel fast multipole accelerated inverse equivalent current method employing Rao-Wilton-Glisson discretization of electric and magnetic surface currents," *IEEE Trans. Antennas Propag.*, vol. 57, no. 4, pp. 1178–1185, Apr. 2009.
[19] Ismatullah and T. Eibert, "Investigation of antenna pattern synthesis through higher order inverse equivalent current method," in *Proc. Eur. Conf. Antennas Propag.*, Apr. 2010, pp. 1–5.
[20] T. Huschka, "Ray tracing models for indoor environments and their computational complexity," in *Proc. 5th IEEE Int. Symp. Personal, Indoor Mobile Radio Commun.*, Sep. 1994, vol. 2, pp. 486–490.
[21] D. Schobert and T. Eibert, "A multilevel interpolating fast integral solver with fast Fourier transform acceleration," in *Proc. URSI Int. Sym. Electromagn. Theory*, Aug. 2010, pp. 520–523.
[22] D. Didascalou, T. Schäfer, F. Weinmann, and W. Wiesbeck, "Ray-density normalization for ray-optical wave propagation modeling in arbitrarily shaped tunnels," *IEEE Trans. Antennas Propag.*, vol. 48, no. 9, pp. 1316–1325, Sep. 2000.
[23] H. Buddendick and T. Eibert, "Efficient multi-aspect RCS simulations based on the shooting and bouncing rays technique," in *Proc. Eur. Conf. Antennas Propag.*, Mar. 2009, pp. 2062–2066.
[24] V. Mohtashami and A. Shishegar, "A new double-counting cancellation technique for ray tracing using separation angle distribution," in *Proc. IEEE Int. RF Microw. Conf.*, Dec. 2008, pp. 306–310.
[25] R. Harrington, *Time-Harmonic Electromagnetic Fields*. New York: IEEE Press, 2001.

Robert Brem (S'11) received the Dipl.-Ing. degree in electrical engineering and information technology from the Technische Universität München, Munich, Germany, in 2010.

He is currently working at the Institute for High-Frequency Engineering, Technische Universität München, as a Research Assistant where his activities include the modeling of antennas, wave propagation, and MIMO systems.

Thomas F. Eibert (S'93–M'97–SM'09) received the Dipl.-Ing.(FH) degree from Fachhochschule Nürnberg, Nuremberg, Germany, in 1989, the Dipl.-Ing. degree from Ruhr-Universität Bochum, Bochum, Germany, in 1992, and the Dr.-Ing. degree from Bergische Universität Wuppertal, Wuppertal, Germany, in 1997, all in electrical engineering.

From 1997 to 1998, he was with the Radiation Laboratory, Electrical Engineering and Computer Science Department, University of Michigan, Ann Arbor. He was with Deutsche Telekom, Darmstadt, Germany from 1998 to 2002, and from 2002 to 2005, he was with the Institute for High-frequency Physics and Radar Techniques, FGAN e.V., Wachtberg, Germany, where he was Head of the Department of Antennas and Scattering. From 2005 to 2008, he was a Professor for radio frequency technology at Universität Stuttgart, Stuttgart, Germany. Since October 2008, he has been a Professor for high-frequency engineering at the Technische Universität München, Munich, Germany. His major areas of interest are numerical electromagnetics, wave propagation, measurement techniques for antennas and scattering, as well as all kinds of antenna and microwave circuit technologies for sensors and communications.